Sun *et al. Earth, Planets and Space* (2018) 70:85
https://doi.org/10.1186/s40623-018-0832-6

Earth, Planets and Space

FULL PAPER

Open Access

El Niño–Southern Oscillation effect on quasi-biennial oscillations of temperature diurnal tides in the mesosphere and lower thermosphere

Yang-Yi Sun[1*], Huixin Liu[1], Yasunobu Miyoshi[1], Libo Liu[2,3] and Loren C. Chang[4,5]

Abstract

In this study, we evaluate the El Niño–Southern Oscillation (ENSO) signals in the two dominant temperature diurnal tides, diurnal westward wavenumber 1 (DW1) and diurnal eastward wavenumber 3 (DE3) on the quasi-biennial oscillation (QBO) scale (18–34 months) from 50 to 100 km altitudes. The tides are derived from the 21-year (January 1996–February 2017) Ground-to-Topside model of Atmosphere and Ionosphere for Aeronomy (GAIA) temperature simulations and 15-year (February 2002–February 2017) Thermosphere Ionosphere Mesosphere Energetics and Dynamics (TIMED)/Sounding of the Atmosphere using Broadband Emission Radiometry (SABER) temperature observations. The results show that ENSO warm phases shorten the period (~ 2 years) of the QBO in DW1 amplitude near the equator and DE3 amplitude at low latitudes of the Northern Hemisphere. In contrast, the QBO period lengthens (~ 2.5 years) during the ENSO neutral and cold phases. Correlation analysis shows the long-lasting effect of ENSO on the tidal QBO in the mesosphere and lower thermosphere.

Keywords: El Niño–Southern Oscillation, Quasi-biennial oscillation, Diurnal tides

Introduction

The El Niño–Southern Oscillation (ENSO) is a planetary-scale ocean–atmosphere-coupled phenomenon (e.g., Trenberth 1997) that affects global climate and weather systems across spatial and temporal scales (e.g., Diaz and Markgraf 2000; Sarachik and Cane 2010). Recent studies have suggested that the ENSO is a significant source of tidal variability in the mesosphere and lower thermosphere (MLT) (Gurubaran et al. 2005; Lieberman et al. 2007; Pedatella and Liu 2012, 2013; Warner and Oberheide 2014). These tides can be modulated by tropospheric forcing and have been suggested as a driver for the ionospheric dynamo (e.g., Jin et al. 2011; Yamazaki and Richmond 2013; Liu 2016b). Gurubaran et al. (2005) first discovered a correlation between interannual variability of low-latitude MLT tides and the ENSO warm phase in 1997/1998. They suggested that large-scale convective systems originating over the western Pacific region in response to the ENSO facilitate excitation of nonmigrating tides through latent heat release or large-scale redistribution of water vapor. Lieberman et al. (2007) reported that the diurnal tides observed at Hawaii and Christmas Island exhibit a pronounced "spike" in amplitude from late 1997 to early 1998 and also speculated that this variability may be linked to the ENSO warm phase. Based on Whole Atmosphere Community Climate Model (WACCM) simulations, Pedatella and Liu (2012, 2013) suggested that the diurnal westward wavenumber (DW1) (1), diurnal eastward wavenumber (DE2) (2), diurnal eastward wavenumber (DE3) (3), and semidiurnal westward wavenumber (SW4) (4) in the lower thermosphere at 110 km respond strongly to the ENSO from November to April. Warner and Oberheide (2014) presented variability of tidal harmonics of the latent heating from 2002 to 2011 associated with the ENSO and found

*Correspondence: yysun0715@gmail.com
[1] Department of Earth and Planetary Science, Kyushu University, Fukuoka 819-0395, Japan
Full list of author information is available at the end of the article

that the nonmigrating tidal response to ENSO is largest during the winter months of 2010/2011.

Numerous studies have also reported that the ENSO controls the stratospheric quasi-biennial oscillation (QBO) through the interactions of broadband atmospheric waves and mean flows (e.g., Taguchi 2010; Geller et al. 2016; Newman et al. 2016; Das and Pan 2016; Christiansen et al. 2016). The deep convection and latent heat release in the tropics are source processes for broadband atmospheric waves, such as Rossby, Kelvin, and gravity waves (Dunkerton 1997; Baldwin et al. 2001). Taguchi (2010) statistically analyzed the stratospheric zonal wind data archive of radiosonde observations at equatorial stations from 1953 to 2008 and found that the change in QBO amplitude between La Niña and El Niño conditions corresponds to about 9% of the grand mean. In contrast, the phase progression rate for the ENSO cycle changes as much as 26% compared to the grand mean. Broadband waves also drive for the QBO above 80 km altitude (Baldwin et al. 2001). Possible ENSO signals with temporal scales longer than one year in the thermosphere (Liu 2016a) and ionosphere (Pedatella and Forbes 2009) have also been reported.

One challenge for exploring the ENSO signal with periods longer than one year in the MLT region is that the QBO and ENSO share a similar period band, which makes them difficult to distinguish using a time series with a limited duration (Warner and Oberheide 2014). The challenge motivates us to analyze longer datasets, including the 21-year GAIA (Ground-to-Topside model of Atmosphere and Ionosphere for Aeronomy) simulations and the 15-year Thermosphere Ionosphere Mesosphere Energetics and Dynamics (TIMED)/Sounding of the Atmosphere using Broadband Emission Radiometry (SABER) observations, and study the response of the MLT tides to the ENSO on a quasi-biennial scale. The two dominant diurnal tides, DW1 and DE3, and the equatorial zonal winds are analyzed in this study.

Data and methodology

The 21-year (January 1996–February 2017) simulations of temperature and zonal wind at altitudes of 50–100 km from the self-consistent GAIA (Jin et al. 2011; Liu et al. 2017) were employed in this study. GAIA consists of a whole atmospheric general circulation, ionospheric, and electrodynamics models. Fields from the Japanese 25-year Reanalysis meteorological data in the troposphere and lower stratosphere (below 30 km) were assimilated into the model to drive the simulations (Jin et al. 2012). In the GAIA database, the latitude–longitude resolution is 2.0° latitude by 2.5° longitude; the vertical spacing is 10 km between 0 and 650 km altitude; and the temporal resolution is 30 min. GAIA has previously been employed to study the effect of the lower atmosphere on the upper atmosphere (e.g., Jin et al. 2012; Liu et al. 2013; Miyoshi et al. 2017).

The 15-year (February 2002–February 2017) thermospheric temperature observations from SABER instrument aboard the TIMED spacecraft were also employed here. SABER provides continuous temperature soundings between 10 and 110 km altitudes within 50°S and 50°N geographic latitudes (Remsberg et al. 2008). The TIMED/SABER data were binned into 2.5° latitude for the tidal computation.

The tidal amplitudes were fitted from the temperature values (F) at each latitude grid using the linear least-squares method (Wu et al. 1995) with the following basis function:

$$F(\lambda,t)=\overline{F}+\sum_{n=1}^{3}\sum_{s=-4}^{4}\widehat{F}_{n,s}cos\left(n\Omega t-s\lambda-\widehat{\psi}_{n,s}\right) \quad (1)$$

where $\widehat{F}$ and $\widehat{\psi}$ are the tidal amplitude and phase. $\overline{F}$ is the zonal mean value. n and s are the tidal harmonic and zonal wave number (westward negative), respectively. Then, $\Omega=\frac{2\pi}{24}h^{-1}$, in which λ and t are longitude and universal time, respectively. The tides from GAIA were estimated monthly. The tides from SABER were estimated from the data collected with a 60-day window, which moved monthly through the period of 2002–2017. The tidal fitting was conducted separately at each 10 km altitudinal grid for both the observation and simulation.

Wavelet analysis (Torrence and Compo 1998) was applied to show the overall temporal variation features in the tidal amplitudes at low latitudes and equatorial zonal mean zonal wind on various scales. A band-pass filter (Matlab fir1) with cutoff periods ranging from 18 to 34 months (Xu et al. 2009) was applied to extract the quasi-biennial oscillation component from the tidal amplitudes and zonal wind. The Oceanic Niño Index (ONI), which is the 3-month running mean of sea surface temperature anomalies in the Niño 3.4 region (5°N–5°S, 120°–170°W), was chosen as a proxy for the ENSO phases (http://www.cpc.noaa.gov/products/analysis_monitoring/ensostuff/ensoyears.shtml). The U30 index is the zonally averaged wind at 30 mb over the equator from the CDAS Reanalysis data (http://www.cpc.ncep.noaa.gov/data/indices/) and represents the stratospheric QBO at 30 mb pressure level (Naujokat 1986).

Results

Figure 1 shows the year-to-year variability in amplitudes of temperature DW1 (diurnal westward wavenumber 1) and DE3 (diurnal eastward wavenumber 3) from GAIA and SABER at 100 km altitude. The GAIA and SABER DW1 is pronounced within 10°S–10°N and its seasonal

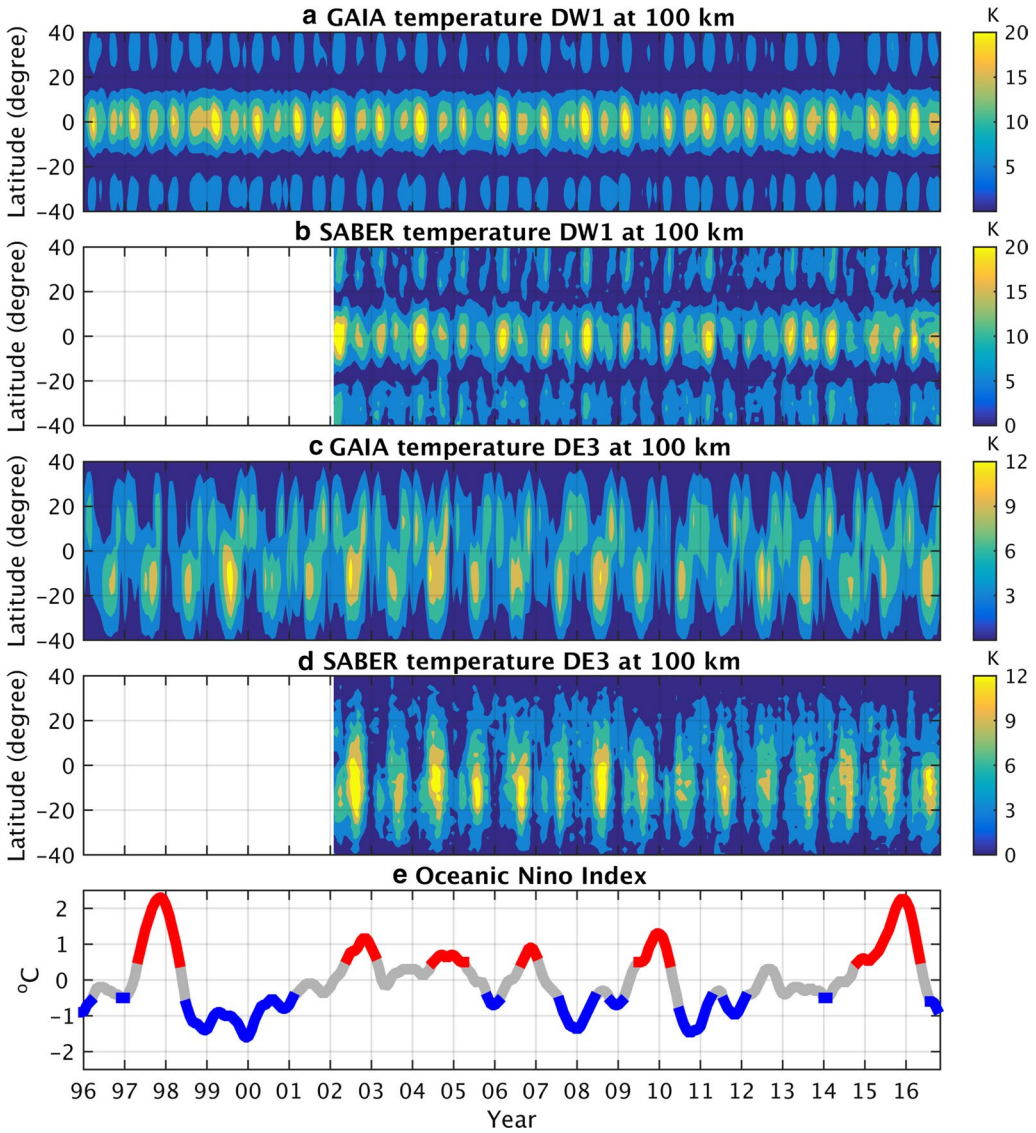

Fig. 1 Amplitude of the two dominant diurnal tides DW1 (diurnal westward wavenumber 1) and DE3 (diurnal eastward wavenumber 3) from GAIA and TIMED/SABER temperature at an altitude of 100 km. (Bottom) Red and blue (exceeding the threshold of ± 0.5 °C) on the Oceanic Niño Index (ONI) indicate the ENSO (El Niño–Southern Oscillation) warm and cold phases

variation reaches maxima near March and August. The DE3 amplitudes from both GAIA and SABER maximize in the Sothern Hemisphere (0°–20°S) near August. In the Northern Hemisphere, the GAIA DE3 amplitude reaches maxima near January and is stronger than that from SABER. Oberheide and Forbes (2008) applied the Hough Mode Extension to analyze temperature and wind measurements from SABER and TIDI (TIMED Doppler Interferometer) in the mesosphere and lower thermosphere region. They presented seasonal DE3 variations in terms of symmetric and antisymmetric modes at various altitudes. The difference between the two DE3 temperature amplitudes (Fig. 1) is due to the presence of the antisymmetric mode in the GAIA DE3 at 100 km altitude. The temporal scales of these clear variations in the DW1 and DE3 amplitudes are near or shorter than 1 year.

ENSO controls the stratospheric QBO, which in turn affects the tidal variation in the MLT region (e.g., Hagan et al. 1999; Forbes et al. 2008; Oberheide et al. 2009; Gan et al. 2014). Correlation analysis is a traditional method that can be applied to detect ENSO signals in the atmosphere (Calvo et al. 2008 and references therein). Accordingly, the correlation analysis has been applied to detect the ENSO signal in the tidal QBOs at altitudes from 50 to

100 km. We note that, as described in "Data and methodology" section, a band-pass filter was applied to extract the tidal QBO embedded in those short-period signals from the amplitudes. However, the correlation between the ONI and QBOs of DW1 and DE3 is low (data not shown). Das and Pan (2016) also reported a low correlation between the Niño 3.4 index and equatorial zonal mean zonal wind in the stratosphere from 1979 to 2013 and suggested that ENSO and QBO are not linearly related. The ENSO signals are not easily isolated from the QBO. Usually, anomalies of a parameter can be defined as departures from the mean cycle with a constant period (e.g., annual mean cycle). However, it is difficult to derive the amplitude anomaly of the QBO by using traditional way due to its flexible period.

A wavelet analysis was further applied to examine the QBO period in detail. The wavelet power spectra (Fig. 2) show that the signal with a period near 2 years is a strong component in the DW1 and DE3 amplitude at 100 km altitude. Gan et al. (2014) also reported that the spectra of the DW1 and DE3 amplitudes from the extended Canadian Middle Atmosphere Model and SABER peak at a period near 25 months. The DW1 QBO is intense over the equator, but the DE3 QBO is stronger in the Northern Hemisphere (0° to 20°N) than that in the Southern Hemisphere (0° to 20°S). Figure 3 shows a time series comparison of the periods for the tidal QBO and QBO-scale component in ONI. The periods of the QBOs in DW1 and DE3 in the Northern Hemisphere transit from ~ 2.5 years to ~ 2 years between 2001 and 2003 and from ~ 2 years to ~ 2.5 years between 2006 and 2008. A similar period transition can be found in the ONI.

The stratospheric QBO can affect the tidal variation in the MLT region (e.g., Hagan et al. 1999; Forbes et al. 2008; Oberheide et al. 2009; Gan et al. 2014). Diurnal tides interact with the zonal mean zonal wind fields in the MLT (Miyahara 1978; McLandress 2002; Miyoshi et al. 2017). Accordingly, Fig. 4 shows the wavelet spectra of the equatorial zonal mean zonal wind from GAIA at 100 km (in lower thermosphere) (Fig. 4a) and 60 km (in mesosphere) (Fig. 4b) as well as the U30 index (in stratosphere) (Fig. 4c). The QBO components in zonal wind mingle with fluctuating short-period signals such as the annual variation in the MLT. In Fig. 4d, the QBO periods at the three altitudes consistently change from ~ 2.5 years to ~ 2 years near 2002 and from ~ 2 years to ~ 2.5 years near 2008. The period transition can be found from the QBOs in the zonal mean zonal wind and tidal DW1 amplitude at various altitude from 50 km to 100 km (Additional file 1: Figs. S1, S2, and S4). The transition is most significant in DE3 QBO at 100 km altitude (Additional file 1: Figs. S3 and S5).

The left panels in Fig. 5 show the time series of the QBO periods in the GAIA zonal mean zonal wind, DW1, and DE3 at altitudes from 50 km to 100 km. The time series of the QBO period is obtained from the wavelet spectra of the GAIA zonal mean zonal wind (Additional file 1: Fig. S1), DW1 (Additional file 1: Fig. S2), and DE3 (Additional file 1: Fig. S3). The periods for both the tidal and zonal wind QBOs are short (~ 2 years) from 2003 to 2007. That duration contains three ENSO warm and one ENSO cold phases. By contrast, the QBO periods are longer (~ 2.5 years) in the 1999–2001 and 2008–2013 durations. Within the two durations, only one ENSO warm phase occurred in 2009/2010, while three strong ENSO cold phases occurred over the remaining time.

The weaker DW1 near the stratopause (~ 50 km) over the equator (Pancheva and Mukhtarov 2011) and the significant QBO phase shift near 70–80 km (Huang et al. 2008) result in an obscuration of the QBO period transitions in zonal mean zonal wind and DW1. It is difficult to detect the period transition in DE3 QBO below 100 km because there the DE3 QBO is much weaker than the short-period components, such as the annual variation. Significant changes in the DE3 asymmetric mode at various altitudes (Oberheide and Forbes 2008) can also disturb the DE3 QBO. The agreement between the QBO period transitions at the various altitudes reveals that ENSO controls the QBO periods in both the stratosphere and MLT.

The right panels in Fig. 5 show the correlation between the periods of the GAIA tidal/zonal wind QBO and the QBO-scale component in ONI. The correlation coefficients have the highest value (correlation coefficient ~ 0.8) when a 1–2 years lead on the ONI corresponding to the QBO is taken into account. They highly correlate (> 0.7) with each other within 3 years after the ENSO occurred. The relationship reveals that the QBO periods take more than 1 year to fully respond to the ENSO. Note that the correlation between two time series with a few periods can be high even while they are uncorrelated. Longer observations collected by ground-based radars or future satellite missions are required to comprehensively examine the period variation of QBOs in the MLT tides.

Discussion and conclusion

The QBO period transition as shown in Figs. 2, 3, 4 and 5 agree with the statistical results presented by Taguchi (2010), wherein the stratospheric QBO period changes from a grand mean of approximately 28 months to 32 and 25 months for the La Niña and El Niño conditions, respectively. Christiansen et al. (2016) also utilized the EC-Earth climate model with sea surface temperature to simulate the stratospheric QBO propagating downward faster during warm ENSOs than during cold ENSOs. A

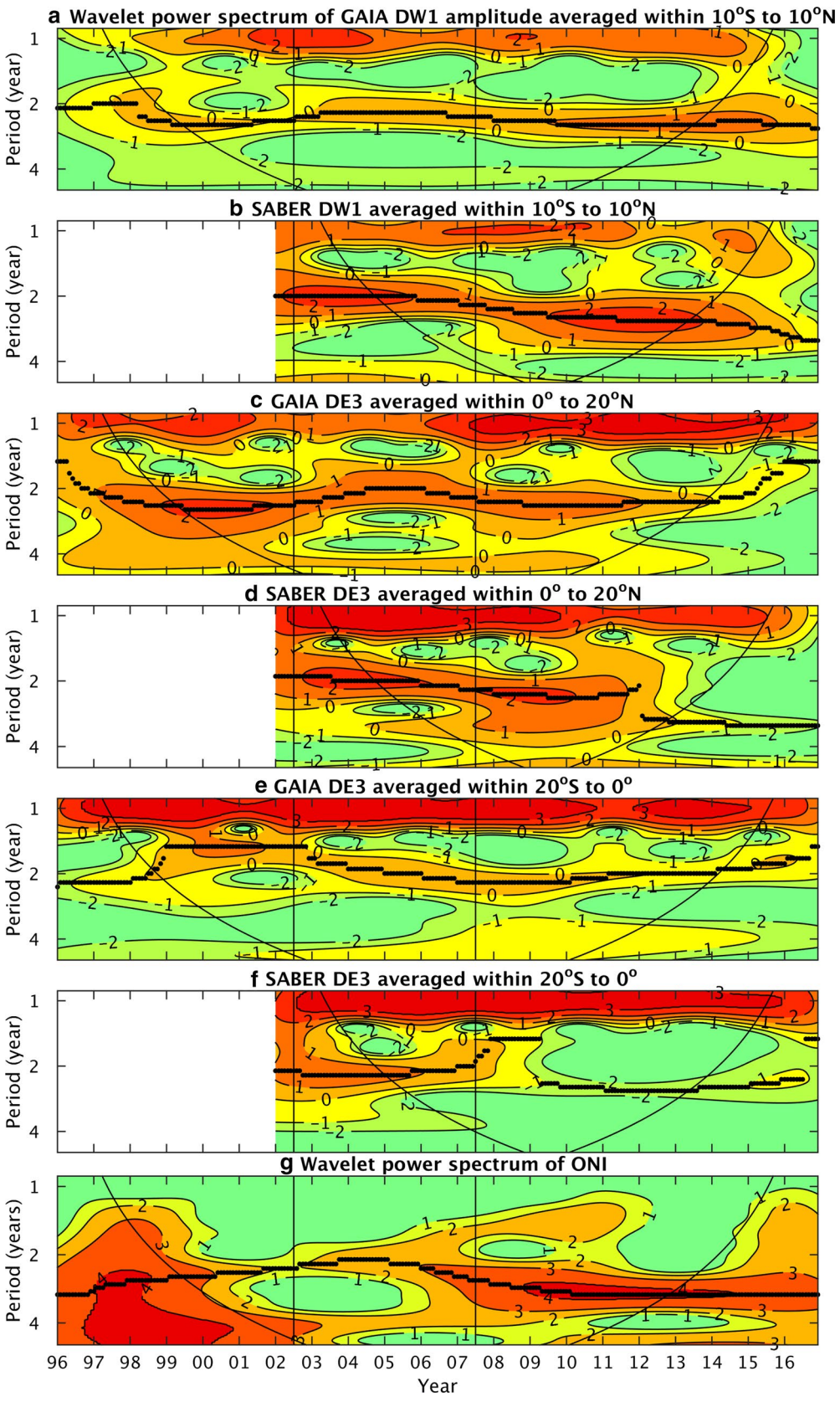
a Wavelet power spectrum of GAIA DW1 amplitude averaged within 10°S to 10°N
b SABER DW1 averaged within 10°S to 10°N
c GAIA DE3 averaged within 0° to 20°N
d SABER DE3 averaged within 0° to 20°N
e GAIA DE3 averaged within 20°S to 0°
f SABER DE3 averaged within 20°S to 0°
g Wavelet power spectrum of ONI
Period (year)
Period (years)
1
2
4
96 97 98 99 00 01 02 03 04 05 06 07 08 09 10 11 12 13 14 15 16
Year

(See figure on previous page.)
Fig. 2 Wavelet power spectra of **a**, **b** the DW1 amplitude averaged within 10°S–10°N, **c**, **d** the DE3 amplitude averaged within 0°–20°N, **e, f** the DE3 amplitude averaged within 0°–20°S, and **g** ONI. The division of DE3 into the two latitudinal regions is due to its equatorial asymmetry natural. The powers are shown on the log2 scale. Black dots indicate the QBO period as a function of time. The QBO period is defined as the location of maximum values, the period ranging from 1.5 to 3.5 years. Black curves indicate the cone of influence zone of the wavelet analysis

causal relationship between the ENSO-induced broadband atmospheric waves, such as Rossby, Kelvin, and gravity waves (Dunkerton 1997; Baldwin et al. 2001), and interaction between the waves and background mean fields has been proposed (e.g., Lindzen and Holton 1968; Das and Pan 2016; Newman et al. 2016). The equatorial tropopause takes 1 to 2 months to respond to El Niño through the convection process (Sun et al. 2014 and references therein). The correlation analysis for the QBO periods (right panels in Fig. 5) reveals that the effect of an ENSO event on the QBOs in the stratosphere and MLT can last more than 1 year through the wave-mean flow interaction. Diurnal tides can be affected by the ENSO when they vertically propagate through the middle atmosphere (e.g., Oberheide et al. 2009; Miyoshi et al. 2017). The cause of the ENSO signal in the zonal wind QBO near 100 km as due to dissipation or breaking of the DW1 (Miyahara 1978) can be further studied.

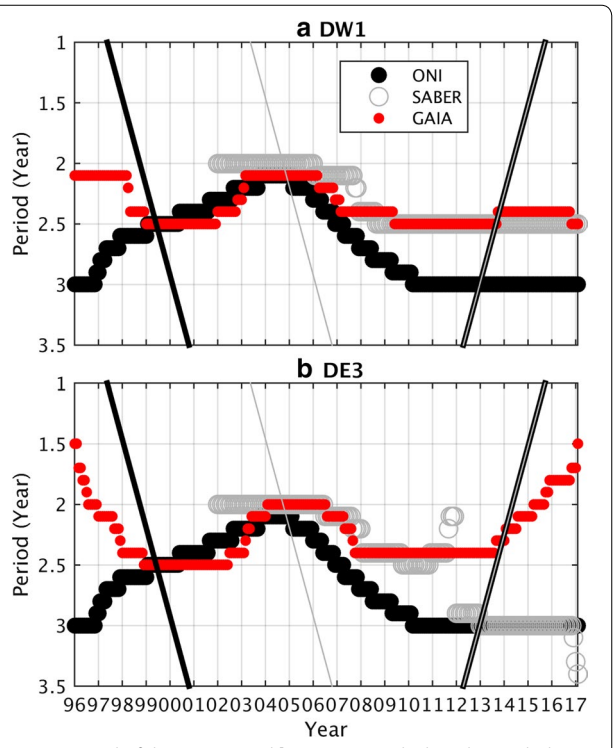

Fig. 3 Period of the **a** DW1 and **b** DE3 QBOs. Black and gray slashes indicate the cone of influence zone for GAIA and SABER, respectively

The intense DW1 and DE3 QBOs from GAIA between 1997 and 1999 correspond to a strong ENSO warm phase in 1997/1998 (top two panels of Fig. 3). Gurubaran et al. (2005) examined MLT radar observations of the diurnal tide at 86 km over Jakarta (6.4°S, 106.7°E) and Tirunelveli (8.7°N, 77.8°E). They found that the annual cycle is relatively weaker between 1996 and 1998, clearly indicating an interannual variability in the diurnal tide. The diurnal tide anomalies over the two stations are correlated with the outgoing longwave radiation anomalies over the western Pacific region (120°E). The interannual variability in the diurnal tide observed by the MLT radars confirms intense QBOs of DW1 and DE3 from GAIA between 1997 and 1999. In comparison, the wavelet spectra for both the GAIA and SABER DW1 (top two panels of Fig. 2) show an enhancement of tidal amplitudes, with a period ranging from 1 to 1.5 years between 2014 and 2016. This period is clearly shorter than the QBO period (18 to 34 months) employed in this study. The wavelet spectra of the GAIA zonal wind, and the U30 index (Fig. 4) also display an enhancement of signals with a period near 1.5 years between 2014 and 2016. The Fourier spectra (in the Additional file 1: Figs. S6–9) show that the zonal wind and DW1 amplitude with period near 1.5 year is significant in the stratosphere and MLT between 2014 and 2016. The agreement suggests responses of the stratosphere, mesosphere and lower thermosphere to the ENSO warm phase of 2014/2016.

A physical-based model can simulate regular phenomena (e.g., QBO) but usually cannot reproduce extreme anomalies (e.g., the enhancement with a period from 1 to 1.5 years between 2014 and 2016). GAIA is a data assimilation system (Jin et al. 2012), where the data assimilation analysis is a compromise between a model simulation and observations (Sun et al. 2015). Therefore, GAIA successfully simulates a shortening of the DW1 QBO during the 2014/2016 ENSO warm phase.

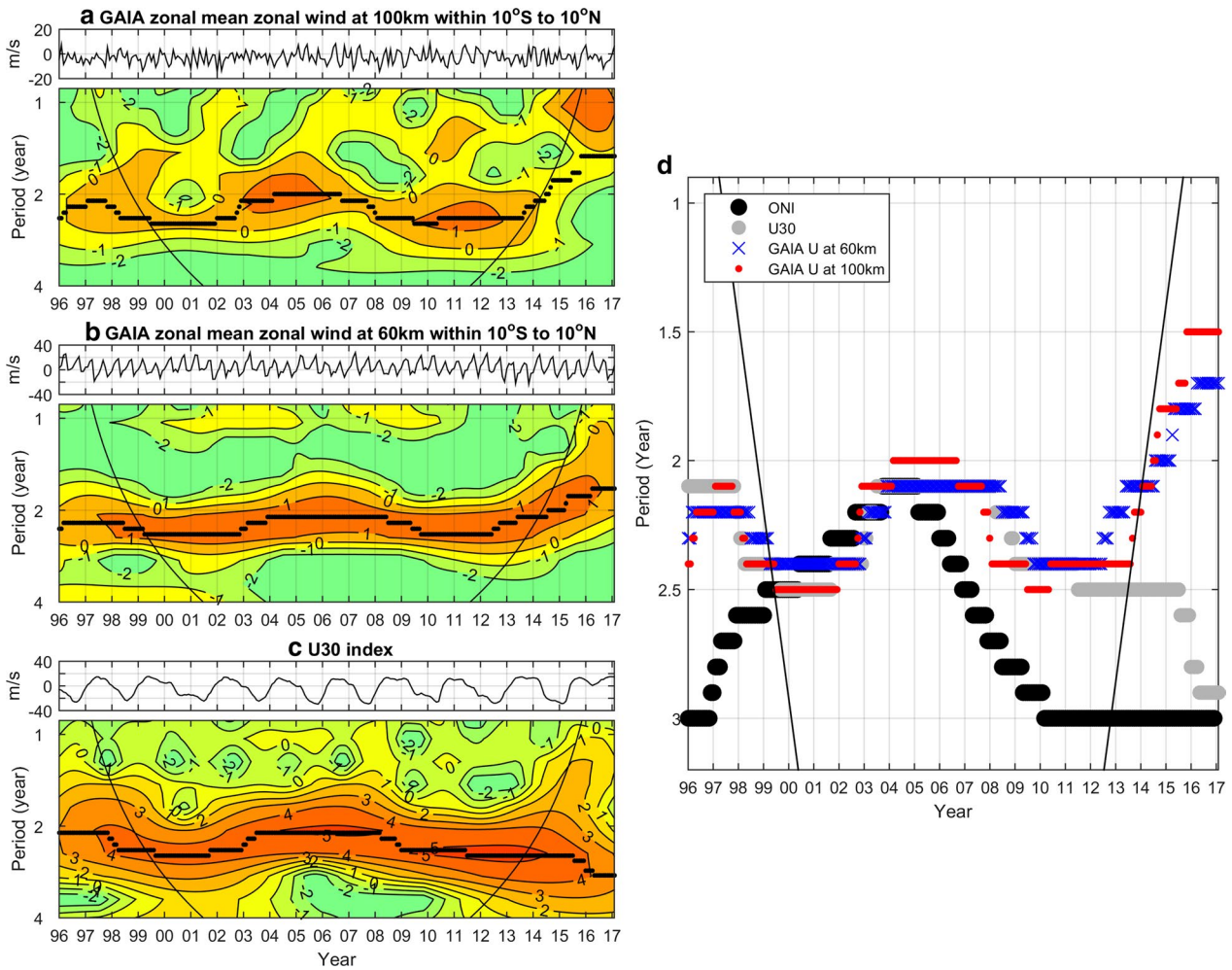

Fig. 4 Wavelet power spectra of the GAIA zonal mean zonal wind averaged within 10°S to 10°N at **a** 100 km and **b** 60 km altitudes. **c** Spectrum of the U30 index. The U30 index is the zonally averaged winds at 30 mb over the equator from the CDAS Reanalysis data. It represents the stratospheric QBO at 30 mb altitude. **d** Periods of the U30 index and QBOs in the GAIA zonal mean zonal wind at altitudes of 60 and 100 km

In conclusion, the GAIA simulations and SABER observations show that the ENSO controls not only the stratospheric QBO, but also the QBO components in the tidal amplitude and zonal mean zonal wind in the mesosphere and lower thermosphere. The QBO process is one of the ways by which the ENSO signal can pass through and reach the lower thermosphere. The QBO periods are close to 2 years and 2.5 years during the ENSO warm phases and neutral/ENSO cold phases, respectively. The ENSO effect on QBO periods can last more than one year. The ionospheric electrodynamics and structure driven by DE3 at the lower thermosphere may also contain the effect from the ENSO. However, it is a challenge to extract it in observations under strong solar influences.

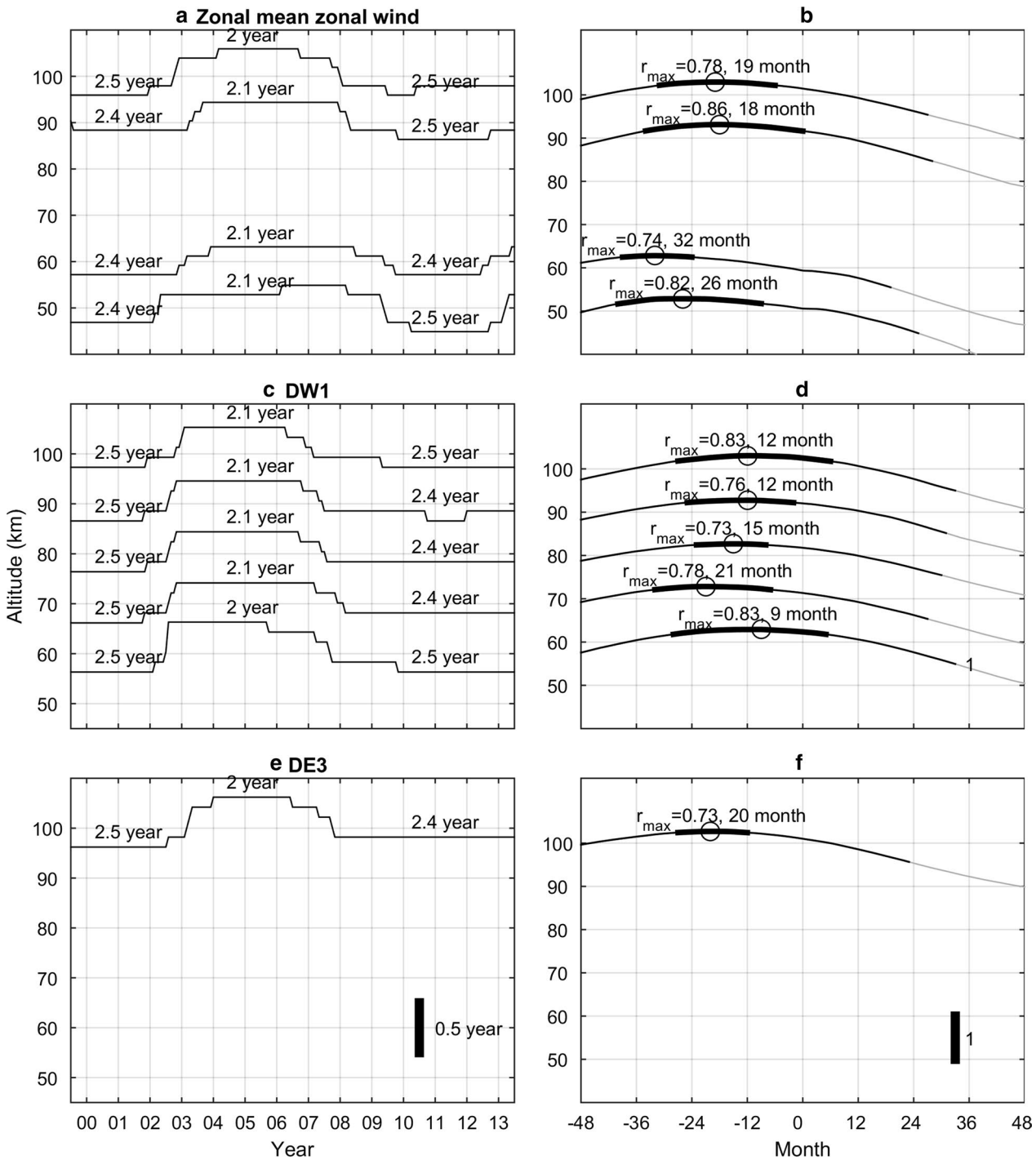

Fig. 5 (Left) Time series of the period of the QBOs in **a** the GAIA zonal mean zonal wind, **c** DW1, and **e** DE3 within the cone of influence zone (from July 1999 to June 2013). The periods are obtained from the wavelet spectra of the zonal wind and tidal amplitude (in the Additional file 1: Figs. S1–3). (Right) Correlation between the periods of the QBO-scale component in ONI and the QBOs from GAIA **b** zonal mean zonal wind, **d** DW1, and **f** DE3 with 99% confidence limit

Additional file

Additional file 1: Figure S1. Time series of GAIA zonal mean zonal wind averaged within 10°S to 10°N at altitudes of **a** 50 km, **b** 60 km, **c** 70 km, **d** 80 km, **e** 90 km, **f** 100 km, and its wavelet power spectra. Black dots indicate the location of maximum values within a period ranging from 1.5 to 3.5 years. **Figure S2.** Time series of GAIA temperature DW1 amplitude averaged within 10°S to 10°N at altitudes of **a** 50 km, **b** 60 km, **c** 70 km, **d** 80 km, **e** 90 km, **f** 100 km, and its wavelet power spectra. Black dots indicate the location of maximum values within a period ranging from 1.5 to 3.5 years. **Figure S3.** Time series of GAIA temperature DE3 amplitude averaged within 0° to 20°N at altitudes of **a** 50 km, **b** 60 km, **c** 70 km, **d** 80 km, **e** 90 km, **f** 100 km, and its wavelet power spectra. Black dots indicate the location of maximum values within a period ranging from 1.5 to 3.5 years. **Figure S4.** Time series of SABER temperature DW1 amplitude averaged within 10°S to 10°N at altitudes of **a** 50 km, **b** 60 km, **c** 70 km, **d** 80 km, **e** 90 km, **f** 100 km, and its wavelet power spectra. Black dots indicate the location of maximum values within a period ranging from 1.5 to 3.5 years. **Figure S5.** Time series of SABER temperature DE3 amplitude averaged within 0° to 20°N at altitudes of **a** 50 km, **b** 60 km, **c** 70 km, **d** 80 km, **e** 90 km, **f** 100 km, and its wavelet power spectra. Black dots indicate the location of maximum values within a period ranging from 1.5 to 3.5 years. **Figure S6.** Fourier spectra of DW1 amplitude and zonal wind from 2014 to 2016. Enhancement of GAIA temperature DW1 with a period close to 1.5 years during the 2014/2016 ENSO warm phase. **a** Fourier spectra of GAIA temperature DW1 amplitude averaged between 10°S and 10°N at various altitudes from 2014 to 2016. **b** Fourier spectra for the period of 2011 to 2013. **c** Altitudinal variation in the amplitude of the signal with the period of 1.5 years. **d** Relative difference between the two amplitude profiles as shown in **e**. **Figure S7.** Same as **Figure S6** but for the SABER temperature DW1 amplitude between 10°S and 10°N. **Figure S8.** Same as **Figure S6** but for the GAIA zonal mean zonal wind between 10°S and 10°N. **Figure S9. a** Fourier spectra of the U30 index from 2014 to 2016 and 2011 to 2013. **b** The difference between the two spectra shows an enhancement of the signal with a period close to 1.5 years.

Abbreviations

ENSO: El Niño–Southern Oscillation; QBO: quasi-biennial oscillation; DW1: diurnal westward wavenumber 1; DE2: diurnal eastward wavenumber 2; DE3: diurnal eastward wavenumber 3; SW4: semidiurnal westward wavenumber 4; GAIA: Ground-to-Topside model of Atmosphere and Ionosphere for Aeronomy; TIMED: Thermosphere Ionosphere Mesosphere Energetics and Dynamics; SABER: Sounding of the Atmosphere using Broadband Emission Radiometry; TIDI: TIMED Doppler Interferometer; MLT: mesosphere and lower thermosphere; WACCM: Whole Atmosphere Community Climate Model.

Authors' contributions

YS, LH, and YM designed and performed experiments, analyzed data, and drafted the manuscript; YM performed the GAIA simulation. LB encouraged YS to investigate QBO. LCC developed the tidal fitting tool. All authors read and approved the final manuscript.

Author details

[1] Department of Earth and Planetary Science, Kyushu University, Fukuoka 819-0395, Japan. [2] Key Laboratory of Earth and Planetary Physics, Institute of Geology and Geophysics, Chinese Academy of Sciences, Beijing 100029, China. [3] Geoscience School, University of the Chinese Academy of Sciences, Beijing 100049, China. [4] Graduate Institute of Space Science, National Central University, Taoyuan 32001, Taiwan. [5] Center for Astronautical Physics and Engineering, National Central University, Taoyuan 32001, Taiwan.

Competing interests

The authors declare that they have no competing interests.

Availability of data and materials

The GAIA simulations were performed using the computer systems at National Institute of Information and Communications Technology, Japan. The TIMED/SABER Version 2.0 data is available at http://saber.gats-inc.com. The Oceanic Niño Index (ONI) is obtained from http://www.cpc.noaa.gov/products/analysis_monitoring/ensostuff/ensoyears.shtml. The U30 index is downloaded from http://www.cpc.ncep.noaa.gov/data/indices/qbo.u30.index.

Consent for publication

Not applicable.

Ethics approval and consent to participate

Not applicable.

Funding

Y. S. thanks the NICT International Exchange Program for support. H. L. acknowledges support from the JSPS KAKENHI grants 18H01270, 18H04446, and 17KK009. Y. M. was supported by JSPS KAKENHI Grant (B)15H03733. L. C. C. was supported by the MOST 103-2111-M-008-019-MY3 Grant from the Taiwan Ministry of Science and Technology.

Publisher's Note

Received: 17 December 2017 Accepted: 5 April 2018
Published online: 21 May 2018

References

Baldwin MP, Gray LJ, Dunkerton TJ, Hamilton K, Haynes PH, Randel WJ, Holton JR, Alexander MJ, Hirota I, Horinouchi T, Jones DBA, Kinnersley JS, Marquardt C, Sato K, Takahashi M (2001) The quasi-biennial oscillation. Rev Geophys 39:179–229. https://doi.org/10.1029/1999RG000073

Calvo N, García-Herrera R, Garcia RR (2008) The ENSO signal in the stratosphere, in trends and directions in climate research. Ann N Y Acad Sci 1146:16–31. https://doi.org/10.1196/annals.1446.008

Christiansen B, Yang S, Madsen MS (2016) Do strong warm ENSO events control the phase of the stratospheric QBO? Geophys Res Lett 43:10489–10495. https://doi.org/10.1002/2016GL070751

Das U, Pan CJ (2016) Equatorial atmospheric Kelvin waves during El Niño episodes and their effect on stratospheric QBO. Sci Total Environ 544:908–918. https://doi.org/10.1016/j.scitotenv.2015.12.009

Diaz H, Markgraf V (2000) El Niño and the Southern Oscillation: multiscale variability and global and regional impacts. Cambridge University Press, Cambridge

Dunkerton TJ (1997) The role of gravity waves in the quasi-biennial oscillation. J Geophys Res 102(D22):26053–26076. https://doi.org/10.1029/96JD02999

Forbes JM, Zhang X, Palo S, Russell J, Mertens CJ, Mlynczak M (2008) Tidal variability in the ionospheric dynamo region. J Geophys Res Space Phys 113:A02310. https://doi.org/10.1029/2007JA012737

Gan Q, Du J, Ward WE, Beagley SR, Fomichev VI, Zhang S (2014) Climatology of the diurnal tides from eCMAM30 (1979 to 2010) and its comparison with SABER. Earth Planet Space. https://doi.org/10.1186/1880-5981-66-103

Geller MA, Zhou T, Yuan W (2016) The QBO, gravity waves forced by tropical convection, and ENSO. J Geophys Res Atmos 121:8886–8895. https://doi.org/10.1002/2015JD024125

Gurubaran S, Rajaram R, Nakamura T, Tsuda T (2005) Interannual variability of diurnal tides in the tropical mesopause region: a signature of the El Niño–Southern Oscillation (ENSO). Geophys Res Lett 32:L13805. https://doi.org/10.1029/2005GL022928

Hagan ME, Burrage MD, Forbes JM, Hackney J, Randel WJ, Zhang X (1999) QBO effects on the diurnal tide in the upper atmosphere. Earth Planet Space 51:571–578. https://doi.org/10.1186/BF03353216

Huang FT, Mayr HG, Reber CA, Russell JM III, Mlynczak MG, Mengel JG (2008) Ozone quasi-biennial oscillations (QBO), semiannual oscillations (SAO), and correlations with temperature in the mesosphere, lower thermosphere, and stratosphere, based on measurements from SABER on TIMED and MLS on UARS. J Geophys Res 113:A01316. https://doi.org/10.1029/2007JA012634

Jin H, Miyoshi Y, Fujiwara H, Shinagawa H, Terada K, Terada N, Ishii M, Otsuka Y, Saito A (2011) Vertical connection from the tropospheric activities to the ionospheric longitudinal structure simulated by a new Earth's whole atmosphere-ionosphere coupled model. J Geophys Res 116:A01316. https://doi.org/10.1029/2010JA015925

Jin H, Miyoshi Y, Pancheva D, Mukhtarov P, Fujiwara H, Shinagawa H (2012) Response of migrating tides to the stratospheric sudden warming in 2009 and their effects on the ionosphere studied by a whole atmosphere-ionosphere model GAIA with COSMIC and TIMED/SABER observations. J Geophys Res 117:A10323. https://doi.org/10.1029/2012JA017650

Lieberman RS, Riggin DM, Ortland DA, Nesbitt SW, Vincent RA (2007) Variability of mesospheric diurnal tides and tropospheric diurnal heating during 1997–1998. J Geophys Res 112:D20110. https://doi.org/10.1029/2007JD008578

Lindzen RS, Holton JR (1968) A theory of the quasi-biennial oscillation. J Atmos Sci 25(6):1095–1107. https://doi.org/10.1175/1520-0469(1968)025<1095:ATOTQB>2.0.CO;2

Liu H (2016a) Thermospheric inter-annual variability and its potential connection to ENSO and stratospheric QBO. Earth Planet Space. https://doi.org/10.1186/s40623-016-0455-8

Liu HL (2016b) Variability and predictability of the space environment as related to lower atmosphere forcing. Space Weather 14:634–658. https://doi.org/10.1002/2016SW001450

Liu H, Jin H, Miyoshi Y, Fujiwara H, Shinagawa H (2013) Upper atmosphere response to stratosphere sudden warming: local time and height dependence simulated by GAIA model. Geophys Res Lett 40:635–640. https://doi.org/10.1002/grl.50146

Liu H, Sun Y, Miyoshi Y, Jin H (2017) ENSO effects on MLT diurnal tides: a 21 year reanalysis data-driven GAIA model simulation. J Geophys Res. https://doi.org/10.1002/2017JA024011

McLandress C (2002) Interannual variations of the diurnal tide in the mesosphere induced by a zonal-mean wind oscillation in the tropics. Geophys Res Lett 29(9):1305. https://doi.org/10.1029/2001GL014551

Miyahara S (1978) Zonal mean wind induced by vertically propagating atmospheric tidal waves in the lower thermosphere. J Meteor Soc Jpn 56:86–97

Miyoshi Y, Pancheva D, Mukhtarov P, Jin H, Fujiwara H, Shinagawa H (2017) Excitation mechanism of non-migrating tides. J Atmos Sol Terr Phys. https://doi.org/10.1016/j.jastp.2017.02.012

Naujokat B (1986) An update of the observed quasi-biennial oscillation of the stratospheric winds over the tropics. J Atmos Sci 43:1873–1877. https://doi.org/10.1175/1520-0469(1986)043<1873:AUOTOQ>2.0.CO;2

Newman PA, Coy L, Pawson S, Lait LR (2016) The anomalous change in the QBO in 2015–2016. Geophys Res Lett 43:8791–8797. https://doi.org/10.1002/2016GL070373

Oberheide J, Forbes JM (2008) Tidal propagation of deep tropical cloud signatures into the thermosphere from TIMED observations. Geophys Res Lett 35:L04816. https://doi.org/10.1029/2007GL032397

Oberheide J, Forbes JM, Haüsler K, Wu Q, Bruinsma SL (2009) Tropospheric tides from 80–400 km: propagation, inter-annual variability and solar cycle effects. J Geophys Res 114:D00105. https://doi.org/10.1029/2009JD012388

Pancheva D, Mukhtarov P (2011) Atmospheric tides and planetary waves: recent progress based on SABER/TIMED. In: Abdu M, Pancheva D (eds) Aeronomy of the Earth's atmosphere and ionosphere, vol 2. IAGA Spec Sopron Book Series. Springer, New York, pp 19–56. https://doi.org/10.1007/978-94-007-0326-1_2

Pedatella NM, Forbes JM (2009) Interannual variability in the longitudinal structure of the low-latitude ionosphere due to the El Niño–Southern Oscillation. J Geophys Res 114:A12316. https://doi.org/10.1029/2009JA014494

Pedatella NM, Liu HL (2012) Tidal variability in the mesosphere and lower thermosphere due to the El Niño–Southern Oscillation. Geophys Res Lett 39:L19802. https://doi.org/10.1029/2012GL053383

Pedatella NM, Liu HL (2013) Influence of the El Niño Southern Oscillation on the middle and upper atmosphere. J Geophys Res Space Phys 118:2744–2755. https://doi.org/10.1002/jgra.50286

Remsberg EE, Marshall BT, Garcia-Comas M, Krueger D, Lingenfelser GS, Martin-Torres J, Mlynczak MG, Russell JM III, Smith AK, Zhao Y, Brown C, Gordley LL, Lopez-Gonzalez MJ, Lopez-Puertas M, She CY, Taylor MJ, Thompson RE (2008) Assessment of the quality of the Version 1.07 temperature-versus-pressure profiles of the middle atmosphere from TIMED/SABER. J Geophys Res 113:D17101. https://doi.org/10.1029/2008JD010013

Sarachik ES, Cane MA (2010) The El Niño–Southern Oscillation phenomenon. Cambridge University Press, Cambridge

Sun YY, Liu JY, Tsai HF, Lin CH, Kuo YH (2014) The equatorial El Niño–Southern Oscillation signatures observed by FORMOSAT-3/COSMIC from July 2006 to January 2012. Terr Atmos Ocean Sci 25:545–558. https://doi.org/10.3319/TAO.2014.02.13.01(A)

Sun YY, Matsuo T, Maruyama N, Liu JY (2015) Field-aligned neutral wind bias correction scheme for global ionospheric modeling at midlatitudes by assimilating FORMOSAT-3/COSMIC *hmF2*data under geomagnetically quiet conditions. J Geophys Res Space Phys 120:3130–3149. https://doi.org/10.1002/2014JA020768

Taguchi M (2010) Observed connection of the stratospheric quasi-biennial oscillation with El Niño-Southern Oscillation in radiosonde data. J Geophys Res 115:D18120. https://doi.org/10.1029/2010JD014325

Torrence C, Compo GP (1998) A practical guide to wavelet analysis. Bull Am Meteorol Soc 79(1):61–78. https://doi.org/10.1175/1520-0477(1998)079<0061:APGTWA>2.0.CO;2

Trenberth KE (1997) The definition of El Niño. Bull Am Meteorol Soc 78(12):2771–2777. https://doi.org/10.1175/1520-0477(1997)078<2771:TDOENO>2.0.CO;2

Warner K, Oberheide J (2014) Nonmigrating tidal heating and MLT tidal wind variability due to the El Niño–Southern Oscillation. J Geophys Res Atmos 119:1249–1265. https://doi.org/10.1002/2013JD020407

Wu DL, Hays PB, Wilbert RS (1995) A least-squares method for spectral-analysis of space-time series. J Atmos Sci 52(20):3501–3511. https://doi.org/10.1175/1520-0469(1995)052<3501:ALSMFS>2.0.CO;2

Xu J, Smith AK, Liu HL, Yuan W, Wu Q, Jiang G, Mlynczak MG, Russell JM III, Franke SJ (2009) Seasonal and quasi-biennial variations in the migrating diurnal tide observed by Thermosphere, Ionosphere, Mesosphere, Energetics and Dynamics (TIMED). J Geophys Res 114:D13107. https://doi.org/10.1029/2008JD011298

Yamazaki Y, Richmond AD (2013) A theory of ionospheric response to upward-propagating tides: electrodynamic effects and tidal mixing effects. J Geophys Res Space Phys 118:5891–5905. https://doi.org/10.1002/jgra.50487